Journal of Magnetism and Magnetic Materials 505 (2020) 166746

Contents lists available at ScienceDirect

Journal of Magnetism and Magnetic Materials

journal homepage: www.elsevier.com/locate/jmmm

Research articles

Structural and magnetic characterization of Al microalloying nanocrystalline FeSiBNbCu alloys

Jiaxin Wu[a,b], Aina He[b], Yaqiang Dong[b], Jiawei Li[b,*], Yunzhuo Lu[a,*]

[a] School of Materials Science and Engineering, Dalian Jiaotong University, Dalian 116028, China
[b] Zhejiang Province Key Laboratory of Magnetic Materials and Application Technology, and CAS Key Laboratory of Magnetic Materials and Devices, Ningbo Institute of Materials Technology & Engineering, Chinese Academy of Sciences, Ningbo, Zhejiang 315201, China

ARTICLE INFO

Keywords:
Nanocrystalline alloys
Magnetic properties
Mössbauer spectroscopy
Magnetic interaction
Annealing process

ABSTRACT

The magnetic properties of nanocrystalline $Fe_{77}Si_{10}B_9Cu_1Nb_{3-x}Al_x$ (x = 0 and 1) alloys have been investigated and their structural and electromagnetic parameters have been quantitatively studied by X-ray diffraction, transmission electron microscopy and Mössbauer spectra under one-step and two-step annealing processes. The nanocrystalline structure consists of single α-Fe(Si) phase embedded in a residual amorphous phase. Both saturation magnetic flux density (B_s) and permeability (μ) of the nanocrystalline alloys are increased by substituting 1 at% Al for Nb and one-step annealing, from B_s = 1.41 T to 1.47 T and from μ = 18,000 to 23,000 at 1 kHz, respectively. The two-step annealing has little effect on the B_s, coercivity (H_c) and grain size of the nanocrystalline alloys, but greatly improves the μ of the Al-doped alloy, reaching up to 28,000 at 1 kHz. The improved μ can be attributed to the increased magnetic moment and exchange stiffness constant, homogeneous chemical structure and reduced magnetostriction. The Al-doped nanocrystalline alloy with high B_s, high μ, low H_c and good frequency stability are good candidates for magnetic shielding pieces of wireless charging.

1. Introduction

Wireless power transfer (WPT) with the advantages of safe and convenient, has great development potential in various aspects, especially in mobile devices, medical equipment and electric vehicles [1,2]. Nowadays, power transfer through magnetic near-field coupling has become a predominant research direction [3]. A lot of effort has been devoted to enhance the charging efficiency and reduce the weight and size of the WPT system, including the design of magnetic shielding pieces (MSPs), coils and circuits. Specifically, the MSPs can improve the coupling between transmitter and receiver and prevent magnetic leakage. Thus, they are thought to be the key components to improve the charging efficiency and reduce electromagnetic interference of the systems [4,5]. Ferrites are the commonly materials of choice due to their low loss and large availability [6]. However, the intrinsic brittleness, low permeability (μ) and low saturation magnetic flux density (B_s) of ferrites make it difficult to meet the needs of miniaturization and high efficiency of electronic devices [7]. Fe-based nanocrystalline alloys have higher B_s, higher μ, lower coercivity (H_c) and lower core losses than ferrites under 300 kHz [8]. Moreover, Fe-based nanocrystalline ribbon, especially when bonded with tape, is flexible and can be made into various geometries. Therefore, the selection of Fe-based nanocrystalline alloys as MSPs is currently an idea choice for the WPT system. Unfortunately, typical nanocrystalline FeSiBNbCu alloys known as Finemet currently in commercial use have a B_s value of less than 1.25 T.

In view of this, a lot of research has focused on improving the B_s of FeSiBNbCu alloy system [8–11]. In general, increasing Fe content and adding appropriate amount of Co can effectively improve the B_s of the alloy system [9]. However, alloys with high Fe content have poor glass formation ability, low μ and high H_c. In addition, Co addition not only increases the cost of raw materials but also deteriorate the soft magnetic properties [12–14]. Adding other elements such as P, Mo and V can simultaneously improve the glass forming ability and μ but at the expense of reducing B_s [15–18]. The addition of Al in Fe-based nanocrystalline alloys has attracted great interest due to its ability to refine grains, reduce magnetic anisotropy and improve frequency stability [19–26]. For example, in FeSiB(NbMo)Cu alloy system, the partial substitution of Fe or B by Al decreases the magnetic anisotropy and grain size of the system, resulting in lower H_c [19–21]. Besides, the replacement of Nb by Al can slightly increase μ [22]. In Fe(SiB)CuP alloy system, the B_s and H_c can be improved by moderate substitution of Si, B and P by Al owing to the formation of a high volume fraction of nanocrystalline α-Fe phase and the decrease of magnetostriction and

* Corresponding authors.
E-mail addresses: lijw@nimte.ac.cn (J. Li), yunzhuohit@gmail.com (Y. Lu).

https://doi.org/10.1016/j.jmmm.2020.166746
Received 11 December 2019; Received in revised form 27 January 2020; Accepted 12 March 2020
Available online 13 March 2020
0304-8853/

magnetic anisotropy [23,24]. In FeCoSiBNbCu alloy system, Al addition can effectively enhance the thermal stability of μ [25]. However, it is difficult to balance the B_s and soft magnetic properties (μ and H_c) of the Al-doped nanocrystalline alloys. For example, the above alloys with excellent soft magnetic properties usually have low B_s (< 1.4 T). To our best knowledge, the Al-doped nanocrystalline alloys with high B_s (> 1.4 T), high μ (> 25,000@1 kHz) and low H_c (< 3 A/m) have not yet been reported, which are the latest requirement for the performance of nanocrystalline alloys for WPT system. Partial substitution of Nb by Al in the Finemet alloys has been found to be an efficient way to increase B_s without deteriorating the soft magnetic properties [22,26]. However, as one of the most important parameters of the MSPs, the μ of the alloys has not been greatly improved. In addition, the influence mechanism of Al microalloying and annealing process on the μ of the alloys is still unclear. In this context, it is very important to optimize the composition and annealing process to simultaneously improve the B_s and μ of the alloys, and reveal the relationship between the magnetic properties and the evolution of microstructure and electromagnetic parameters.

Herein, the effects of Al microalloying in $Fe_{77}Si_{10}B_9Cu_1Nb_{3-x}Al_x$ (x = 0 and 1 at%, hereafter referred to Al_0 and Al_1, respectively) alloys on structural and magnetic properties as a function of annealing process have been investigated in detail. It is found that the 1 at% substitution of Nb by Al and two-step annealing significantly improve the magnetic properties of the alloys, i.e., high B_s of 1.47 T, high μ up to 28,000 and H_c as low as 3 A/m. The change of the magnetic properties is explained in terms of the structural evolution and the magnetic interaction quantified by transmission election microscopy (TEM) and Mössbauer spectroscopy, which also complements previous investigations of Al-doped nanocrystalline alloys.

2. Experimental

$Fe_{77}Si_{10}B_9Cu_1Nb_{3-x}Al_x$ (x = 0 and 1) alloys were prepared by induction-melting mixtures of high pure Fe (99.99%), Si (99.99%), B (99.95%), Nb (99.99%), Cu (99.99%) and Al (99.99%) under purity argon atmosphere. The ribbons with 24 μm thick and 1.1 mm wide were obtained by melt-spinning method with a wheel velocity of 45 m/s in nitrogen. The crystallization temperatures of the melt-spun ribbons were measured by differential scanning calorimetry (DSC, 404C) at a heating rate of 40 K/min under high purity argon flow. Nanocrystalline ribbons were obtained through annealing the melt-spun ribbons in a tubular furnace under vacuum atmosphere. One-step annealing was carried out at 783–883 K for 10 min, while two-step annealing was at 633–693 K and 863 K for 10 min, respectively. The structure characterization of as-spun and annealed samples was investigated by X-ray diffraction (XRD, D8 ADVANCE) with Cu-Kα radiation and TEM (TecnaiF20). The Curie temperatures (T_C) of the amorphous matrix and nanocrystalline alloys were measured with DSC at a heating rate of 40 K/min and differential thermal analysis (TG-DTA) at a heating rate of 10 K/min, respectively. The B_s was measured with a vibrating sample magnetometer (VSM, Lakeshore7410) at room temperature. The H_c was evaluated with a *B-H* loop tracer (EXPH-100) under a field of 800 A/m. The μ under the frequency range from 1 kHz to 110 MHz was examined by a HP4294A impedance analyzer in a field of 1 A/m. Mössbauer spectra was carried out using ^{57}Co/Rh as γ-ray source. Electromagnetic parameters such as isomer shift (*IS*), average magnetic hyperfine field (B_{hf}) and crystallization volume fraction (V_{cry}) were fitted by MossWinn4.0 fitting program.

3. Results and discussion

3.1. Thermal properties

Fig. 1(a) shows the DSC curves of melt-spun ribbons. It is clear that the primary crystallization temperature (T_{x1}) decreases from 754 K for the Al-free alloy (Al_0) to 741 K for the 1 at% Al alloy (Al_1), indicating that the substitution of Nb by Al promotes the precipitation of α-Fe(Si) phase. Also, the secondary crystallization temperature (T_{x2}) decreases from 940 K for Al_0 to 908 K for Al_1. Thus, the crystallization interval between T_{x1} and T_{x2} decreases with the addition of Al, suggesting the decrease in the thermal stability of the alloy. However, the T_C of the amorphous matrix of Al_1 is higher than that of Al_0, indicative of improved ferromagnetic exchange of the amorphous matrix. Based on the DSC results and previous work, two-step annealing process was introduced in order to obtain high volume fraction of α-Fe(Si) grains and inhibit the precipitation of Fe-boride phases [27,28]. As shown in Fig. 1(b), in the first step, the melt-spun ribbons were annealed at T_{a1} for 10 min, and then were cooled to room temperature by water quenching. In the second step, the pre-annealed ribbons were annealed at 863 K (this is the optimal temperature based on our one-step annealing process) for 10 min.

3.2. Magnetic properties

Fig. 2 shows the variations of magnetic properties of Al_0 and Al_1 under different annealing processes. One-step and two-step annealing processes are conveniently labeled as (I) and (II), respectively. Both annealing processes have little influence on the B_s and H_c of the alloys within the error range, but significantly improve the μ of Al_1. The increase in B_s from about 1.41 T for Al_0 to about 1.47 T for Al_1 is as would be expected for the substitution of Nb by Al that has smaller atomic size and mass. With the increase of annealing temperature, the μ of Al_1 increases almost linearly, whereas the μ of Al_0 is roughly unchanged. It is interesting to find that (II) is more beneficial to improve the μ of Al_1 than (I) (22% increase), but has little effect on the μ of Al_0. Besides, Al_1(II) has a maximum μ of 28000, much higher than that (18000) of Al_0(I) and Al_0(II). Moreover, Al_1 exhibits higher frequency stability than Al_0. As shown in Fig. 3(a), the μ of Al_0 decreases linearly with the increase of frequency, whereas the μ of Al_1 has little change below 30 kHz. Normally, the greater the μ, the lower the H_c. However, the H_c of Al_1 is 1 A/m greater than that of Al_0. The phenomenon will be discussed in detail in terms of effective magnetic anisotropy and magnetic interaction in Section 3.4.

3.3. Microstructure analysis

According to the random anisotropy model [8], soft magnetic properties depend on the grain size of nanocrystalline alloys. In order to reveal the influence of Al addition and annealing process on soft magnetic properties, the microstructure of Al_0 and Al_1 was studied by XRD (Fig. 3(b)) and TEM (Fig. 4). As shown in Fig. 3(b), all samples show a nanocrystalline state with a α-Fe(Si) phase embedded in a residual amorphous matrix. No Fe-boride phase can be detected. The half-peak width of the diffraction peaks of Al_1 is higher than that of Al_0 under the same annealing condition, suggesting that Al_1 has larger grain size. TEM analyses confirm the results of XRD. Selected-area electron diffraction (SAED) patterns with a typical nanocrystalline ring further prove the coexistence of α-Fe(Si) and amorphous phases. The average grain sizes *D* and characteristic distribution are shown in the histograms. The somewhat larger grain size of Al_1 may arise from the decrease of thermal stabilty (as evident in Fig. 1(a)), which results in a slight increase in H_c. It is seen that the grain distribution of Al_0(II) is slightly more concentrated and uniform than that of Al_0(I). This may be attributed to the densification of Cu clusters, which promotes the nucleation and inhibits the growth of α-Fe(Si) phase [17,28,29]. However, Al_0(II) has almost the same soft magnetic properties as Al_0(I). By contrary, Al_1(II) has similar grain size and characteristic distribution with Al_1(I), but shows higher μ. Thus, it is difficult to explain the variation of soft magnetic properties in terms of grain size in the present alloy system (note that both TEM and magnetic propertes measurements were repeated for three times).

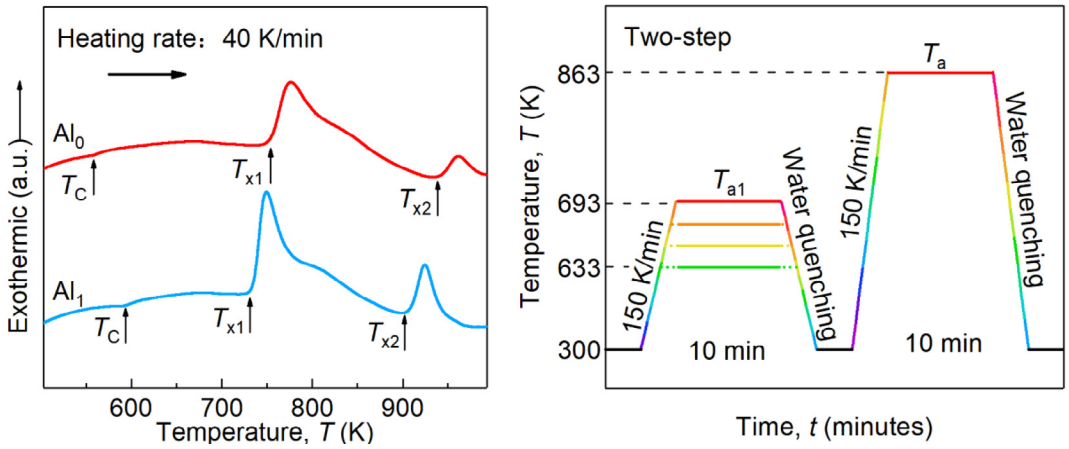

Fig. 1. (a) DSC curves of melt-spun Al_0 and Al_1. (b) Flow chart of time and temperature used for two-step annealing process.

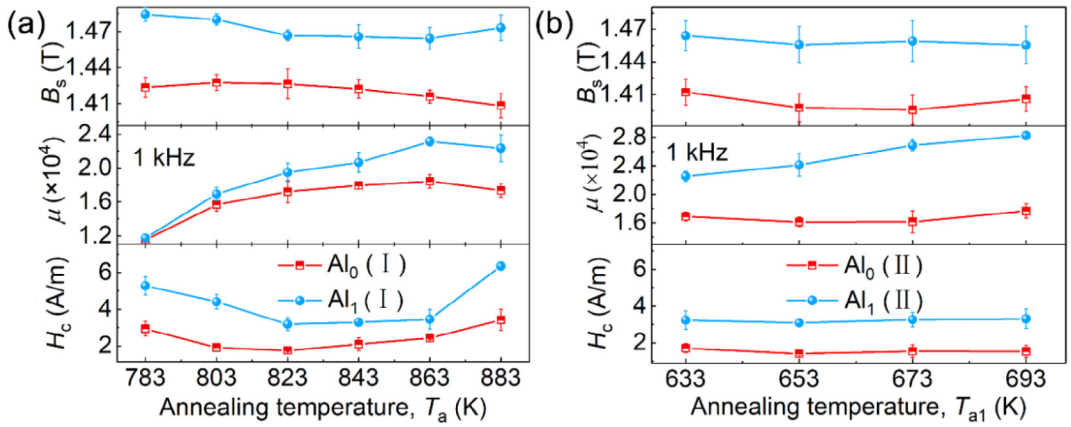

Fig. 2. B_s, μ and H_c of Al_0 and Al_1 as a function of annealing temperature. (a) One-step annealing at T_a; (b) two-step annealing at T_{a1} and 863 K, respectively.

3.4. Mössbauer spectra

As mentioned above, Al microalloying and optimum annealing process can effectively improve the μ of FeSiBNbCu, yet do not refine the grain size and reduce the H_c of the alloy. This result is different from previous work [23,25,30,31]. To reveal the mechanism of the improved μ, we have carried out Mössbauer spectra analysis. As shown in Fig. 5(a), the spectra clearly show six individual sextet components, including amorphous and crystallized α-Fe(Si) phases with DO3 structure. The subspectra of α-Fe(Si) phases correspond to 0Si, 1Si, 2Si, 3Si and 4Si, respectively (Fe atoms have 0-4 nearest-neighbors of Si atoms) [32]. This is consistent with the results of XRD and TEM. However, it is difficult to directly distinguish the spectral variations of the alloys. Therefore, *IS*, B_{hf} and V_{cry} that are the principal parameters of Mössbauer spectra have been investigated and given in Table 1. *IS* relates to the density of *s*-electrons in Fe nucleus. The absolute value of *IS* in Al_1 is smaller than that in Al_0, indicating that the *s*-electron charge density at Fe-sites in Al_1 is enhanced [33]. This is because the nearest sites of Fe atoms are occupied by a small amount of Al atoms, which also leads to the diversification of nanocrystalline and higher degree of crystallization (Table 1). On one hand, Al is preferentially solubilized into α-Fe crystals during crystallization compared with amorphous matrix [34].

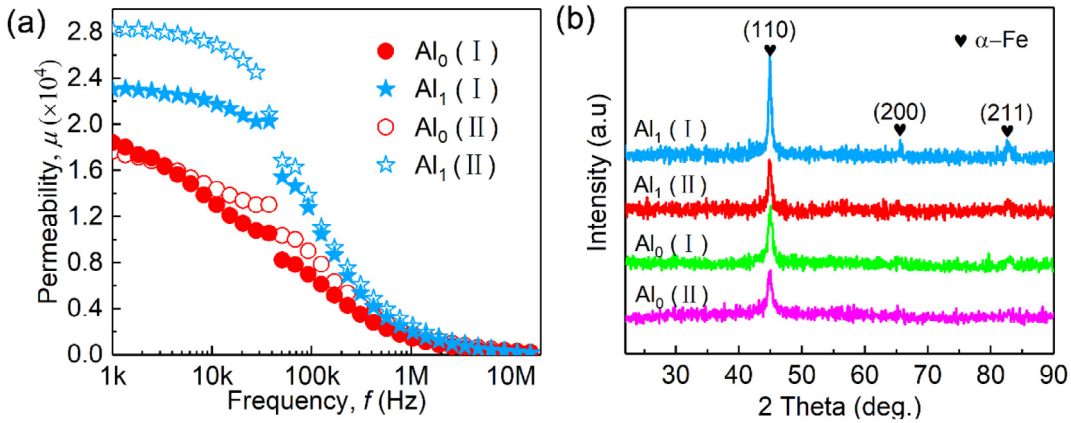

Fig. 3. (a) Dependence of μ on frequency and (b) XRD of Al_0 and Al_1. (I): annealing at 863 K for 10 min; (II): annealing at 693 K and 863 K for 10 min, respectively.

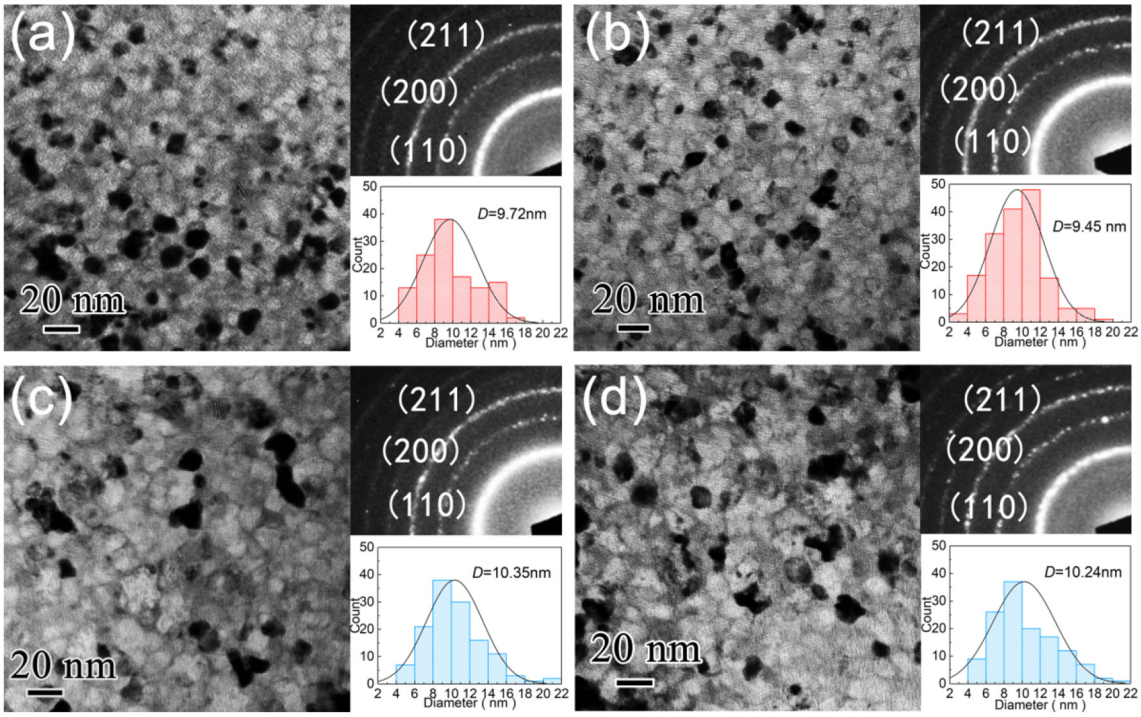

Fig. 4. TEM micrographs, SAED images and characteristic grain size distribution of (a) Al_0(I), (b) Al_0(II), (c) Al_1(I) and (d) Al_1(II).

On the other hand, the reduction of Nb in the amorphous matrix weakens its inhibition on the diffusion of Fe atoms [35]. B_{hf} can reflect the exchange interaction between Fe atoms, which is approximately linear with the magnetic moment of Fe atoms [36,37]. The B_{hf} of Al_1 is larger than that of Al_0, conforming that Al_1 has a higher magnetic moment and thus shows higher B_s. Since the volume fraction of amorphous matrix reaches about 40%, the amorphous matrix also affects the soft magnetic properties of the alloys. The magnetic hyperfine field of amorphous matrix (B_{hf}^a) are 16.91 T for Al_0(I), 16.73 T for Al_0(II), 17.56 T for Al_1(I), and 17.48 T for Al_1(II), respectively. Thus, Al_1 has higher B_{hf}^a than Al_0, which may be due to a decrease in Nb and an increase in Fe. The hyperfine field of amorphous matrix distributions are distinctly separated into two areas, that is 8–15 T low field area and

Table 1
Hyperfine parameters of Al_0 and Al_1. (I): annealing at 863 K for 10 min; (II): annealing at 693 K and 863 K for 10 min, respectively. *IS*: isomer shift, B_{hf}^a: magnetic hyperfine field of amorphous matrix, B_{hf}: average magnetic hyperfine field, V_{cry}: crystallization volume fraction.

	IS (mm/s)	B_{hf}^a (T)	B_{hf} (T)	V_{cry} (%)
Al_0 (I)	−0.0690	16.91	23.48	56.51
Al_1 (I)	−0.0647	17.56	23.89	57.88
Al_0 (II)	−0.0728	16.73	23.43	57.75
Al_1 (II)	−0.0611	17.48	23.75	60.53

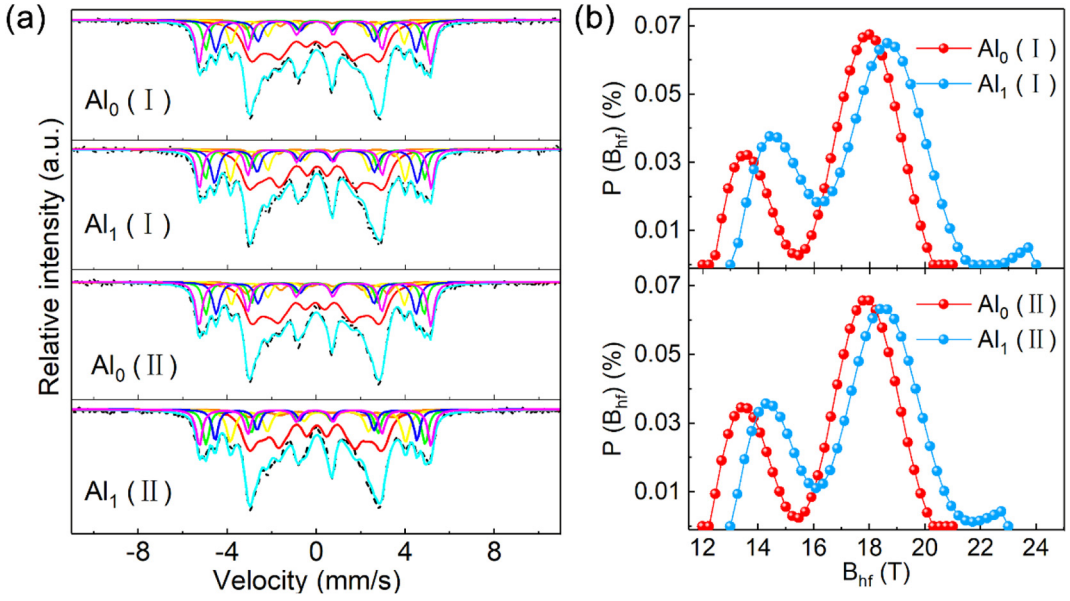

Fig. 5. (a) Mössbauer spectra and (b) corresponding hyperfine field distributions of Al_0 and Al_1 amorphous matrix.

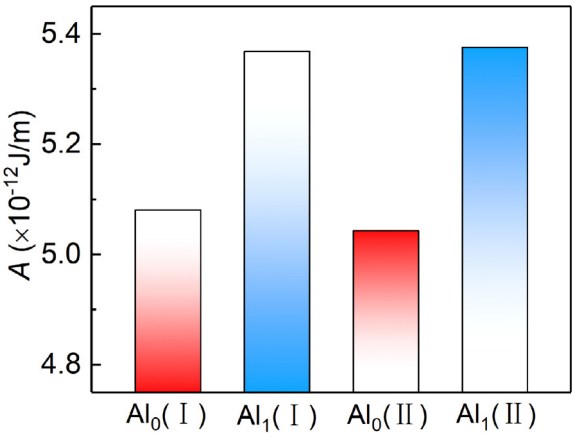

Fig. 6. Exchange stiffness constant A of Al_0 and Al_1.

15–35 T high field area, as showed in Fig. 5 (b). The low field area has weak magnetic interaction due to the enrichment of nonmagnetic B, Cu and Nb atoms in the adjacent shell of Fe atoms, whereas the high field area shows strong magnetic interaction owing to the enrichment of Fe atoms [33,38]. It is found that the peaks of Al_1 shift to higher B_{hf} than that of Al_0, suggesting that the substitution of Nb by Al facilitates Cu and Nb atoms to escape from the first coordination shell of Fe atoms in the structural relaxation process. Thus, the magnetic interaction of Al_1 is improved [39].

The improved μ of Al_1 can be interpreted by the Herzer's model [40]:

$$\mu \propto \frac{M_s^2}{\mu_0\left[\left(\frac{K_1^4 D^6}{A^3}\right)+\left(\frac{3}{2}\,|\lambda_s \sigma|\right)\right]} \tag{1}$$

in which M_s is the saturation magnetization, μ_0 is the vacuum permeability, K_1 is the magneto-crystalline anisotropy of α-Fe(Si), D is the grain size, A is the exchange stiffness constant, λ_s is the saturation magnetostriction and σ is the residual stress.

A can be obtained by Refs. [41] and [42]:

$$A = \frac{x_{Fe} S_{Fe-Fe} k_B T_C}{4(S_{Fe-Fe}) r_{Fe-Fe}} \tag{2}$$

in which x_{Fe} is the concentration of Fe in atomic percent, k_B is the Boltzmann constant, T_C is the Curie temperature of the nanocrystalline alloys, $r_{Fe\text{-}Fe}$ is the nearest-neighbor distance (twice of Fe atomic radius) of Fe atoms, and $S_{Fe\text{-}Fe}$ is the spin moment of Fe atoms, which can be obtained from the following equations:

$$S_{Fe-Fe} = M(\mu_B)/2x_{Fe}\mu_B \tag{3}$$

$$M(\mu_B) = B_s Z/\rho N_A \tag{4}$$

where $M(\mu_B)$ is the magnetic moment of the samples considering Bohr magnetons, μ_B is the Bohr magnetons, Z is the molar mass, ρ is the density and N_A is the Avogadro constant. The T_C of the nanocrystalline alloys are 915 K for Al_0(I), 911 K for Al_0(II), 956 K for Al_1(I), and 960 K for Al_1(II), respectively. It is clear that the annealing process has little effect on T_C. However, the substitution of Nb by Al significantly improves T_C. It is well known that T_C and local atomic moments are positively correlated [9]. Thus, Al_1 with larger magnetic moment shows higher T_C than Al_0. Based on Eqs. (2)–(4), the A of Al_0 and Al_1 are shown in Fig. 6. Although annealing process has little effect on A, Al_1 has greater A than Al_0 due to the higher B_s and T_C. This agrees well with the results of Mössbauer spectra. It is seen from Eq. (1) that the μ is directly proportional to the M_s and A, but is inversely proportional to the D, K_1 and λ_s. As mentioned above, the addition of Al effectively increases the M_s and A due to the increase of magnetic interaction. TEM images display that the D has a slightly increase for Al_1. However, K_1 is considered constant because the contents of Fe and Si of Al_0 and Al_1 have no change. Since Al has been shown to effectively reduce the λ_s of Fe-based alloys [8,43] and Al_1 has a higher V_{cry} than Al_0 (beneficial for further decreasing λ_s) [44], it is reasonable to deduce that Al_1 has a lower λ_s than Al_0. Therefore, the increase in M_s and A as well as the decrease in λ_s make Al_1 have greater μ than Al_0 despite the slightly increase in D. In addition, the change in chemical heterogeneity of amorphous matrix can be evaluated by the relative area of the low field [35]. The smaller the relative area of the low field, the more uniform the amorphous matrix. The relative area of Al_1(II) in the low field is 6.63%, which is smaller than that (8.01%) of Al_1(I). Thus, compared with Al_1(I), the higher V_{cry} and more homogeneous chemical structure may be responsible for the improved μ of Al_1(II).

4. Conclusions

The influence of Al microalloying and annealing process on the magnetic properties and structure of nanocrystalline $Fe_{77}Si_{10}B_9Cu_1Nb_{3-x}Al_x$ (x = 0 and 1) alloys have been shown. The substitution of 1 at% Nb by Al improves the B_s, μ and frequency stability of the nanocrystalline alloys, yet the H_c dose not decrease due to the slightly increased grain size. Although the two-step annealing has little effect on the magnetic properties of Al-free nanocrystalline alloy, it can greatly improve the μ of Al-doped nanocrystalline alloy. The improved μ is mainly due to the enhancement of magnetic moment, exchange stiffness constant and structural uniformity as well as the reduction of magnetostriction. The Al microalloying and two-step annealing make the alloy have excellent magnetic properties, i.e., high B_s of 1.47 T, high μ up to 28,000 and low H_c of 3 A/m, which can meet the performance requirements of nanocrystalline alloys for wireless charging.

Declaration of Competing Interest

The authors declare that they have no known competing financial interests or personal relationships that could have appeared to influence the work reported in this paper.

Acknowledgments

This work was supported by National Key Research and Development Program of China (Grant No. 2016YFB0300500), National Natural Science Foundation of China (Grant No. 51771215), Public Projects of Zhejiang Province (Grant No. LGG20E010003) and Ningbo Major Special Projects of the Plan "Science and Technology Innovation 2025" (Grant No. 2018B10084).

References

[1] P. Machura, Q. Li, A critical review on wireless charging for electric vehicles, Renew. Sustain. Energy. Rev. 104 (2019) 209–234.
[2] G. Kiruthiga, A. Sharmila, P. Mahalakshmi, M. Muruganandam, Power optimisation for wearable heart rate measurement device with wireless charging, J. Med. Eng. Technol. 41 (2017) 288–297.
[3] M.Z. Song, P. Belov, P. Kapitanova, Wireless power transfer inspired by the modern trends in electromagnetics, Appl. Phys. Rev. 4 (2017) 021102.
[4] S. Morita, T. Hirata, E. Setiawan, I. Hodaka, Power efficiency improvement of wireless power transfer using magnetic material, 2nd ICFST,, IEEE, 2017, pp. 304–307.
[5] Y. Urzhumov, D.R. Smith, Metamaterial-enhanced coupling between magnetic dipoles for efficient wireless power transfer, Phys. Rev. B 83 (2011) 205114.
[6] Z. Lin, L. Wang, Z. Huang, Studies on the different assembles of magnetic shielding pieces in electromagnetic induction-type wireless charging system, Appl. Phys. A-Mater. 125 (2019) 114.
[7] D.E. Gaona, T. Long, Feasibility analysis of nanocrystalline cores for polarize and non-polarized IPT charging pads, 34th APEC, IEEE. (2019) 1539–1546.
[8] G. Herzer, Modern soft magnets: Amorphous and nanocrystalline materials, Acta Mater. 61 (2013) 718–734.
[9] M.A. Willard, M. Daniil, Nanocrystalline soft magnetic alloys two decades of progress, Handb. Magn. Mater. 21 (2013) 173–342.
[10] A. Inoue, A. Makino, T. Bitoh, Magnetic properties of nanocrystalline materials, Nanostruct. Mater. 487–536 (2007).

[11] Y. Yoshizawa, Magnetic properties and applicantions of nanostructured soft magnetic materials, Scr. Mater. 44 (2001) 1321–1325.

[12] M. Kuhnt, X.D. Xu, M. Amalraj, P. Kozikowski, K.G. Pradeep, T. Ohkubo, M. Marsilius, T. Strache, C. Polak, M. Ohnuma, K. Hono, G. Herzer, The effect of Co addition on magnetic and structural properties of nanocrystalline (Fe, Co)-Si-B-P-Cu alloys, J. Alloys Compd. 766 (2018) 686–693.

[13] R. Parsons, Z. Li, K. Suzuki, Nanocrystalline soft magnetic materials with a saturation magnetization greater than 2 T, J. Magn. Magn. Mater. 485 (2019) 180–186.

[14] F.L. Kong, C.T. Chang, A. Inoue, E. Shalaan, F. Al-Marzouki, Fe-based amorphous soft magnetic alloys with high saturation magnetization and good bending ductility, J. Alloys Compd. 615 (2014) 163–166.

[15] H. Amano, A. Hasegawa, K. Ara, K. Horino, H. Matsumoto, FeNbBP type nanocrystalline alloy with high B_s of 1.64 T optimized by sputtered thin film method, AIP Adv. 9 (2019) 035027.

[16] J. Xu, Y.Z. Yang, W. Li, X.C. Chen, Z.W. Xie, Effect of P addition on glass forming ability and soft magnetic properties of melt-spun FeSiBCuC alloy ribbons, J. Magn. Magn. Mater. 417 (2016) 291–293.

[17] Y.B. Han, R. Wei, Z.C. Li, F.S. Li, A.T. Wang, C.T. Chang, X.M. Wang, Improvement of magnetic properties for V-substituted $Fe_{73.5}Si_{13.5}B_9Cu_1Nb_{3-x}V_x$ nanocrystalline alloys, J. Mater. Sci: Mater Electron. 28 (2017) 10555–10563.

[18] M. Xiao, Z. Zheng, L. Ji, X. Liu, Z. Qiu, D. Zeng, The role of V and Mo on crystallization process and magnetic properties of FeSiBCuNb alloys using in wide frequency scale, J. Non-Cryst. Solids 521 (2019) 119546.

[19] J. Moya, M. Garcia, M. Vazquez, H. Sirkin, Role of aluminium in structural and magnetic properties of nanocrystalline alloy FeSiBNbCu, J. Phys. IV 8 (1998) 135–138.

[20] I. Todd, B.J. Tate, H.A. Davies, M.R.J. Gibbs, D. Kendall, R.V. Major, Magnetic properties of ultrasoft-nanocomposite FeAlSiBNbCu alloys, J. Magn. Magn. Mater. 215 (2000) 272–275.

[21] H. Duan, Z. Wang, Y. Jia, Al addition effect on structure and magnetic properties in high B_s Fe-Cu-Si-B alloys, Mater. Res. Bull. 111 (2019) 289–293.

[22] H. Liu, C. Yin, X. Miao, Z. Han, D. Wang, Y. Du, Permeability spectra study of $Fe_{73.5}Si_{13.5}B_9Cu_1Nb_{3-x}Al_x$ (x = 0, 0.1, 0.2, 0.4, 0.8 and 1.6), J. Alloys Compd. 466 (2008) 246–249.

[23] F. Shahri, R. Gholamipour, B. Garmeh, Effect of Al on the structure and magnetic properties of nanocrystalline FeSiBPCu melt-spun ribbons, Trans. Indian Inst. Met. 71 (2017) 35–39.

[24] J.S. Zhu, Y.G. Wang, G.T. Xia, J. Dai, J.K. Chen, $Fe_{83}P_{15}Cu_1Al_1$ partial nanocrystalline alloy obtained by one-step melt spinning method, J. Alloys Compd. 666 (2016) 243–247.

[25] X. Li, Z. Wang, H.J. Duan, The effect of the minor Al addition on microstructure and soft magnetic properties for $(Fe_{0.5}Co_{0.5})_{73.5}Si_{13.5}Nb_3Cu_1B_9$ nanocrystalline alloy, J. Non-Cryst. Solids 517 (2019) 114–118.

[26] Z.J. Yan, B.R. Bian, Y. Hu, S.E. Dang, L.T. Xia, Y.M. Wang, Influence of Al and Ni on the magnetic properties of Finemet alloys, J. Magn. Magn. Mater. 322 (2010) 3359–3362.

[27] Y. Han, A. Wang, A. He, C. Chang, F. Li, X. Wang, Improvement of magnetic properties, microstructure and magnetic structure of $Fe_{73.5}Cu_1Nb_3Si_{15.5}B_7$ nanocrystalline alloys by two-step annealing process, J. Mater. Sci: Mater Electron. 27 (2015) 3736–3741.

[28] G.T. Xia, Y.G. Wang, J. Dai, Y.D. Dai, Effects of Cu cluster evolution on soft magnetic properties of $Fe_{83}B_{10}C_6Cu_1$ metallic glass in two-step annealing, J. Alloys Compd. 690 (2017) 281–286.

[29] K.G. Pradeep, G. Herzer, P. Choi, D. Raabe, Atom probe tomography study of ultrahigh nanocrystallization rates in FeSiNbBCu soft magnetic amorphous alloys on rapid annealing, Acta Mater. 68 (2014) 295–309.

[30] B.S. Dong, S.X. Zhou, M.J. Hu, W.Z. Chen, B.L. Shen, The influence of Al content on glass forming ability and magnetic properties of high M_s nanocrystalline FeSiBPCuAl alloy, Mater. Lett. 64 (2010) 736–738.

[31] J.S. Zhu, Y.G. Wang, Effect of Al addition on the glass forming ability, thermal stability and soft magnetic properties of $(Fe_{0.83}P_{0.16}Cu_{0.01})_{100-x}Al_x$ nanocrystalline alloys, J. Alloys Compd. 652 (2015) 220–224.

[32] M.I. Oshtrakh, Z. Klencsár, V.A. Semionkin, E. Kuzmann, Z. Homonnay, L.K. Varga, Annealed FINEMET ribbons: Structure and magnetic anisotropy as revealed by the high velocity resolution Mössbauer spectroscopy, Mater. Chem. Phys. 180 (2016) 66–74.

[33] C.D. Stanciu, J.B. Marimon da Cunha, I. Chicinaş, O. Isnard, Structural, magnetic and Mössbauer spectroscopy characterisation of the Fe-15 wt%Si nanocrystalline powder obtained by mechanical alloying and annealing, J. Alloys Compd. 797 (2019) 865–873.

[34] P.J. Warren, I. Todd, H.A. Davies, A. Cerezo, M.R.J. Gibbs, D. Kendall, R.V. Major, Partitioning behaviour of Al in a nanocrystalline $Fe_{71.5}Si_{13.5}B_9Nb_3Cu_1Al_2$ alloy, Scr. Mater. 41 (1999) 1225–1227.

[35] C. Cao, Y. Wang, L. Zhu, Y. Meng, X. Zhai, Y. Dai, J. Chen, F. Pan, Local structure, nucleation sites and crystallization behavior and their effects on magnetic properties of $Fe_{81}Si_xB_{10}P_{8-x}Cu_1$ (x = 0–8), Sci. Rep. 8 (2018) 1243.

[36] N. Zhang, G. Li, X. Wang, T. Liu, J. Xie, The influence of annealing temperature on hyperfine magnetic field and saturation magnetization of Fe–Si–Al–Cr flake-shaped particles, J. Alloys Compd. 672 (2016) 176–181.

[37] S.M. Dubiel, Relationship between the magnetic hyperfine field and the magnetic moment, J. Alloys Compd. 488 (2009) 18–22.

[38] T. Szumiata, B. Górka, A. Zorkovská, P. Sovák, Structure and hyperfine interactions in Al-doped Finemet, J. Magn. Magn. Mater. 295 (2005) 95–105.

[39] P. Gupta, A. Gupta, A. Shukla, T. Ganguli, A.K. Sinha, G. Principi, A. Maddalena, Structural evolution and the kinetics of Cu clustering in the amorphous phase of Fe-Cu-Nb-Si-B alloy, J. Appl. Phys. 110 (2011) 033537.

[40] G. Herzer, Soft magnetic nanocrystalline materials, Scr. Metall. Mater. 33 (1995) 1741–1756.

[41] R. Hasegawa, R.J. Gambino, J.J. Cuomo, J.F. Ziegler, Effect of thermal annealing and ion radiation on the coercivity of amorphous Gd–Co films, J. Appl. Phys. 45 (1974) 4036–4040.

[42] W. Yang, H. Liu, L. Xue, J. Li, C. Dun, J. Zhang, Y. Zhao, B. Shen, Magnetic properties of $(Fe_{1-x}Ni_x)_{72}B_{20}Si_4Nb_4$ (x = 0.0–0.5) bulk metallic glasses, J. Magn. Magn. Mater. 335 (2013) 172–176.

[43] R. Zuberek, C. Miguel, J. González, P. García-Tello, G.R. Aranda, T. Kulik, H. Szymczak, Investigations of effective magnetic anisotropy and magnetostriction of amorphous and nanocrystalline $Fe_{71.5}Cu_1Nb_3Al_2Si_{13.5}B_9$ alloy by FMR, Mater. Sci. Eng. A 375–377 (2004) 1173–1176.

[44] Y. Jin, Y. Chao, F. Liu, J. Wang, M. Sun, Nanocrystallization and magnetostriction coefficient of $Fe_{52}Co_{34}Hf_7B_6Cu_1$ amorphous alloy treated by medium-frequency magnetic pulse, J. Magn. Magn. Mater. 468 (2018) 181–184.